

Article

# Hydricity of 3d Transition Metal Complexes from Density Functional Theory: A Benchmarking Study

Alister S. Goodfellow  and Michael Bühl \* 

School of Chemistry, University of St Andrews, St Andrews KY16 9ST, UK; ag266@st-andrews.ac.uk

\* Correspondence: buehl@st-andrews.ac.uk

**Abstract:** A range of modern density functional theory (DFT) functionals have been benchmarked against experimentally determined metal hydride bond strengths for three first-row TM hydride complexes. Geometries were found to be produced sufficiently accurately with RI-BP86-D3(PCM)/def2-SVP and further single-point calculations with PBE0-D3(PCM)/def2-TZVP were found to reproduce the experimental hydricity accurately, with a mean absolute deviation of 1.4 kcal/mol for the complexes studied.

**Keywords:** DFT; 3d metal complex; benchmark; hydricity



**Citation:** Goodfellow, A.S.; Bühl, M. Hydricity of 3d Transition Metal Complexes from Density Functional Theory: A Benchmarking Study. *Molecules* **2021**, *26*, 4072. <http://doi.org/10.3390/molecules26134072>

Academic Editors: William T. A. Harrison, R. Alan Aitken and Paul Waddell

Received: 3 June 2021

Accepted: 30 June 2021

Published: 3 July 2021

**Publisher's Note:** MDPI stays neutral with regard to jurisdictional claims in published maps and institutional affiliations.



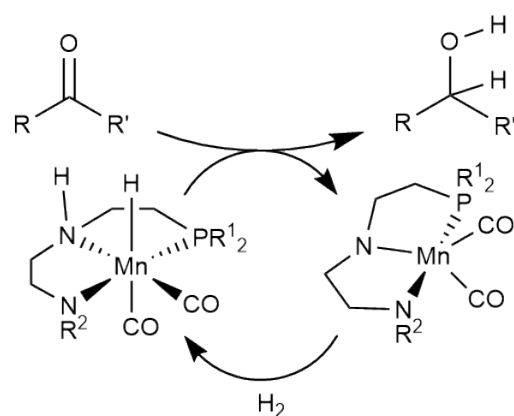
**Copyright:** © 2021 by the authors. Licensee MDPI, Basel, Switzerland. This article is an open access article distributed under the terms and conditions of the Creative Commons Attribution (CC BY) license (<https://creativecommons.org/licenses/by/4.0/>).

## 1. Introduction

At the forefront of modern chemistry is sustainability, with a drive towards 'greener' processes and development. Catalysis has always been a tool used to reduce energetic costs and to promote specific reactions, improving selectivity and the efficacy of various transformations. Traditionally, homogeneous catalysts have been based upon expensive and unsustainable metals such as platinum, palladium and rhodium [1] and while these 4d and 5d transition metals (TMs) have been very successful in this application, their future use is limited by concerns over sustainability and price. The scarcity of the metals has resulted in a high economic and social cost in their extraction. The metals themselves are also toxic, which may lead to issues of contamination in extraction, chemical transformations, or in the application of these catalysts in industrial processes. To alleviate these issues, development has moved towards the use of 3d TMs, which are largely more abundant, less toxic and more sustainable [2–5].

First-row TM catalysts have undergone huge development in the past few years and are being optimised to ultimately become competitive against their unsustainable heavy metal congeners. Iron and manganese are attractive due to their low toxicity and high abundance, and work on catalytic hydrogenation reactions using these metals is very topical (see Scheme 1). For a review on the development of manganese based pincer catalysts, see Garbe et al. [6].

Density functional theory is a powerful tool for the elucidation of reaction mechanisms and for the rational design of these catalytic systems. To accurately study such systems, the DFT functional used must be suitable for the system, accurately predicting bond energies that are crucial to the functionality of the molecule. 3d TMs are notoriously tricky to study with DFT, especially bare TMs where the electronic structure is not always predicted correctly [7,8]. For investigation in the field of homogeneous catalysis, especially in hydrogenation reactions as shown in Scheme 1, the metal hydride bond will be of prime importance for the catalytic activity, and the functional used must be accurate in the description of these bond strengths.



**Scheme 1.** A representation of the catalytic application of Mn-based systems from the group of Beller [9].

A number of papers have used DFT computations to examine the reactivity of these catalytic systems and a variety of methodology has been employed (Table 1). The choice of methodology may be based upon previous work in related catalysis, perhaps 4d metal systems, or simply by using methods that have already been applied in the literature. For example, early computations from the Beller group used B3PW91, based upon the performance of this hybrid functional in previous work (including benchmarking studies) across 3d, 4d and 5d transition metal complexes though more recent work from this group has used the hybrid PBE0 functional [9–15].

An alternate approach was adopted by Ge et al. [16], where the methodology was selected based upon the testing of a range of functionals for a multi-step transformation. M06 was selected for their work as the computed barrier heights were found to be closest to the average value across the functionals tested. A benchmarking study was performed by Gamez et al. [17] on a number of high-spin Mn-based complexes using a range of different functionals. It was found that pure functionals (i.e., non-hybrid) favoured low-spin forms of these Mn complexes, with weak-field nitrogen and oxygen based ligands, experimentally known to be high-spin complexes. B3LYP was found to produce poor geometries and PBE0 was recommended for use on these systems. Dispersion corrections were also found to be of importance in optimisation. The accurate description of spin states is important in the study of 3d metal complexes, where the energetic splitting of metal-based 3d orbitals may be small and multi-state reactivity may be possible.

**Table 1.** A summary of the literature methodology used for DFT calculations on 3d metal catalytic systems.

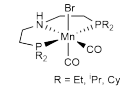
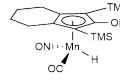
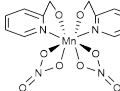
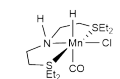
System	Methodology <sup>a</sup>	Dispersion <sup>b,c</sup>	Solvent Model <sup>c</sup>	References
 R = Et, Pr, Cy	B3PW91/TZVP			[9,10,15]
	M06/6-31++G(d,p)	M	PCM	[16]
	PBE0/def2-TZVP			[17]
	$\omega$ B97X-D/ECP (Mn)/6-31++G(d,p)	GD2	PCM	[18]

Table 1. Cont.

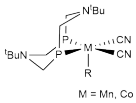
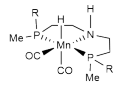
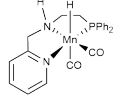
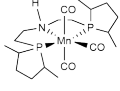
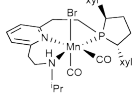
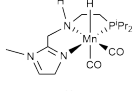
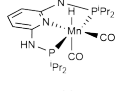
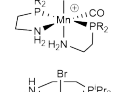
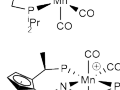
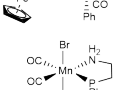
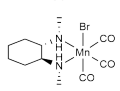
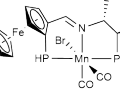
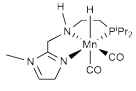
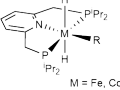
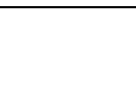
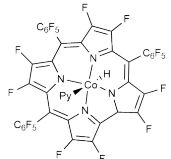
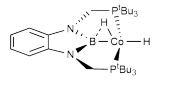
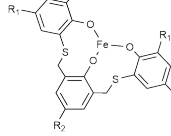
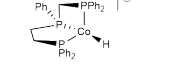
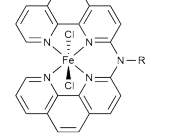
System	Methodology <sup>a</sup>	Dispersion <sup>b,c</sup>	Solvent Model <sup>c</sup>	References
 M = Mn, Co	M06/ECP (Mn,Co)/6-31(+G(d,p)	M	PCM	[19]
	$\omega$ B97X-D/ECP (Mn)/cc-PVTZ	GD2	PCM	[20]
	M06/TZVP// $\omega$ B97X-D/TZVP (Mn)/SVP	M sp GD2 opt	PCM	[21]
	B3PW91/TZVP			[22]
	$\omega$ B97X-D/ECP (Mn)/cc-pVDZ	GD2	PCM	[23]
	M06L/def2-TZVP// B3LYP/def2-SVP	M sp	SMD sp	[24]
	PBE0/ECP (Mn)/6-31G(d,p)		PCM	[25]
	PBE0/6-311+G(d,p)// PBE0/6-31G(d,p)			[26]
	DSD-PBE96-NL/def2-QZVP// PBE0-D3/def2-TZVP	GD3BJ opt		[27]
	M06/6-311++G(d,p)// M06/ECP (Mn)/6-31G(d)	M	SMD sp	[28]
	PBE0/6-311+G(d)// PBE0/6-31G(d)		PCM sp	[29]
	PBE0/def2-QZVPP// PBE0-D3/def2-TZVP	GD3BJ opt	SMD opt	[30]
	PBE0/ECP (Mn)/6-31G(d,p)			[31]
	B3LYP/ECP (Mn)/6-311++G(d,p)		CPCM	[32]
 M = Fe, Co	$\omega$ B97X/6-31++G(d,p)		PCM	[33]

Table 1. Cont.

System	Methodology <sup>a</sup>	Dispersion <sup>b,c</sup>	Solvent Model <sup>c</sup>	References
	BP86/6-311+G(d)// BP86/6-311G(d) (Co)/6-31G(d)		PCM sp	[34]
	B3PW91/ECP (Co)/6-31++G(d,p)// B3PW91/ECP (Co)/6-31++G(d,p) (B,N,P)/6-31G(d)	GD sp GD opt	CPCM sp	[35]
	M06/TZVP// BP86/ECP (Fe)/SVP	M sp	PCM sp	[36]
	B3PW91/def2-TZVP// B3PW91/TZVP	GD3BJ sp	SMD sp	[37]
	B3LYP*/ECP (Fe)/6-311+G(2df,2p)// B3LYP/ECP (Fe)/6-31G(d,p)	GD3BJ sp GD3BJ opt	SMD sp	[38]

<sup>a</sup> For simplicity, the use of any pseudopotential has been indicated with ECP. <sup>b</sup> M denotes that there is implicit dispersion included, due to the parametrisation of the Minnesota family of functionals. GD is used to indicate the inclusion of Grimme's empirical dispersion correction, with BJ denoting the use of Becke-Johnson dampening. <sup>c</sup> 'sp' and 'opt' denote the use of dispersion corrections or solvation models in either the single-point or geometry optimisation calculation, respectively.

We now present a validation study on the performance of these and other functionals for the calculation of hydricity for a few select complexes. Hydricity is the heterolytic bond dissociation energy of a metal hydride to a metal cation and hydride (Equation (1)), predicted to be an important property for the study of hydrogenation catalysis.



A sizeable amount of  $\Delta G_{\text{H}^-}^{\circ}$  data is available from experiment [39], the ultimate benchmark. Arguably, this quantity is key in determining the ease of elementary steps such as transfer of the hydride to an electrophilic substrate (*cf.* upper arrow in Scheme 1). As it turns out, there is a notable variability in the performance of different functionals in their ability to reproduce these hydricity values, and some clear recommendations for functionals to choose can be made.

## 2. Methodology

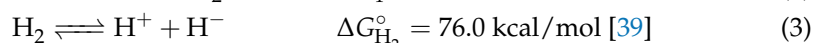
### 2.1. Computational Details

Geometry optimisations were performed primarily at the GGA level of DFT using the BP86 functional, employing a variety of basis sets from the redefinitions of the Ahlrichs family of bases [40–43]. Structures obtained by X-ray crystallography for closely related systems were used as starting points in geometry optimisations [44–46]. This is akin to the methodology of Neale [47] used in the investigation of Fe(II) and Co(III) catalysis and of Bühl and Kabrede [48] in the benchmarking of geometries for a wide range of first-row transition metal complexes. Def2-TZVP was used for the investigations of proton and metal cation solvation and throughout further benchmarking, a variety of basis from this family were used; def2-SVP, with def2-TZVP describing the metal atom of Fe or Co, and the addition of a diffuse function on the hydridic hydrogen, taking 1/3 of the exponent from the diffuse 's' function in the def2-TZVP basis for hydrogen. Dispersion

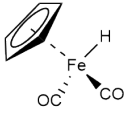
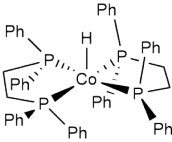
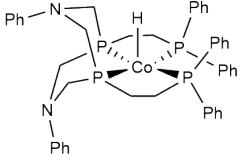
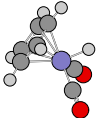
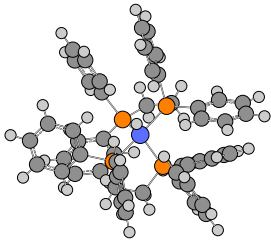
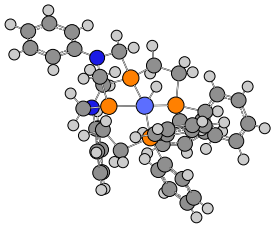
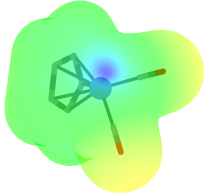
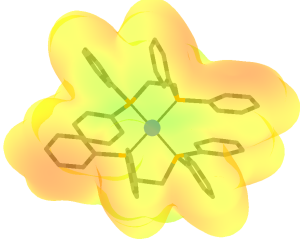
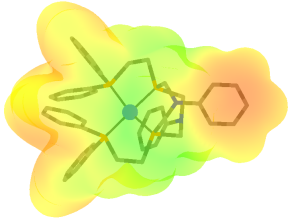
corrections were included throughout, predominantly with the D3 empirical correction from Grimme [49], including Becke-Johnson dampening [50]. Implicit solvation was also included using the Polarizable Continuum Model with the integral equation formalism (IEF-PCM, herein referred to as PCM) employing the parameters of acetonitrile ( $\epsilon = 35.688$ ). The explicit treatment of a small number of individual solvent molecules acting as ligands was also considered (Section 3.1). The nature of the minima obtained were verified by computation of harmonic frequencies at the same level of theory. Single-point energies were obtained using a number of functionals from a range of levels on Jacob's ladder [51] using the def2-TZVP basis, with an ultrafine integration grid (99 radial shells with 590 angular points per shell). The impact of using a larger, quadruple- $\zeta$  basis, def2-QZVP, was also explored. The functionals considered were; B3LYP [52–54], B3PW91 [52,55–57], BLYP [53,54,58], BP86 [58,59], CAM-B3LYP [60], M06 [61], M06-2X [61], M06-HF [62,63], M06-L [64], M11 [65], M11-L [66], MN12-L [67], MN15 [68], MN15-L [69], PBE [55,70], PBE0 [71], PBE0-1/3 [72], revPBE [73], revPBE0 [73], TPSS [74], TPSSh [74,75],  $\omega$ B97X-D [76]. Dispersion was included for all single-point calculations as mentioned earlier, except for the Minnesota family of functionals, which are parametrised to account for dispersion, and the  $\omega$ B97X-D functional includes the D2 correctional term from Grimme [77]. Thermochemistry was evaluated at 468 atm (to mimic bulk acetonitrile, see Section 1 in the ESI for details) and 298.15 K using thermodynamic corrections obtained at the level of the geometry optimisation, combined with single-point energetics. Density fitting, invoking the RI approximation with the Gaussian keyword 'auto', was used where possible for pure functionals. Calculations were performed primarily using Gaussian 09, D.01 [78], with some single-points evaluated using Gaussian 16, C.01 [79] where the functional was unavailable in Gaussian 09. Some geometries were also evaluated using the more recent optimiser of Gaussian 16 to remove spurious imaginary frequencies that could not be removed with Gaussian 09. Where Gaussian 16 was used, defaults from the older Gaussian 09 were employed to ensure that there was no change in implementation across different versions (see Table S5 in the ESI).

## 2.2. Calculation of Hydricity

To determine a functional suitable for the study of 3d TM catalysts (for example, see Scheme 1), we have chosen to benchmark three 3d TM hydride complexes, for which there are experimentally determined hydricity values ( $\Delta G_{\text{H}^-}$ , Table 2) [39]. Direct evaluation of hydricity according to Equation (1) is challenging computationally. In this work we use a thermodynamic cycle with a protonation as key step, where the ionic stoichiometry is maintained across the reaction (i.e. charge separation is avoided, Equation (2)). This has been done to ensure that there is no artefact arising from an imbalance of ionic species, as their large stabilisation in a polar solvent is difficult to compute accurately using methods employing implicit solvation, such as PCM (as would be the case by directly modelling Equation (1)). By combination with  $\text{H}_2$  heterolysis obtained from experiment [39] (Equation (3)), the thermochemical cycle may be completed to obtain the thermodynamic hydricity.



**Table 2.** Three 3d transition metal complexes with experimentally determined thermodynamic hydricity values ( $\Delta G_{H^-}$ ).

Complex	FeCp(CO) <sub>2</sub> H	Co(dppe) <sub>2</sub> H	Co(P <sub>4</sub> N <sub>2</sub> )H
$\Delta G_{H^-}$ (kcal/mol)	61.7 [39,80]	49.9 [81,82]	31.8 [82]
			
			
Positively charged cationic complex fragment after hydride dissociation <sup>a</sup>			

<sup>a</sup> Hydrogen atoms have been removed for clarity. The viewing angle is looking towards the vacant site on the metal centre where the hydridic hydrogen atom was residing previously, emphasising the accessibility of the now vacant site by a solvent molecule. Electron density (isodensity value of 0.001 a.u.) mapped with electrostatic potential [colour-coded between 0.00 a.u. (red) and +0.35 a.u. (blue)].

With limited availability of Mn based data, neutral Co and Fe hydride complexes have been chosen from data by Wiedner et al. [39] as representatives of 3d metal hydride systems. Benchmarking studies have previously been performed on 3d TM diatomics [83], but the applicability of these studies to such larger complexes remains unclear.

### 2.3. Acetonitrile Proton Clusters

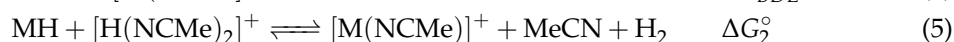
The proton involved in Equation (2) will be modelled through a complex with discrete solvent molecules. Experimentally, acetonitrile had been used as a solvent and it was observed by Himmel et al. [84] that, in acetonitrile, proton-solvent clusters were present in the form of extended hydrogen bonded arrays,  $[H(NCMe)_n]^+$ , with values of  $n$  up to 8. For the purpose of this study, we determined that the proton-solvent cluster was suitably described with two explicit solvent molecules ( $n = 2$ ) forming an inner solvent shell and approximation of the outer solvent shell with implicit solvation using a polarisable continuum model (further details are available in Section 2 of the ESI).

## 3. Results and Discussion

### 3.1. Explicit Treatment of Solvent Molecules

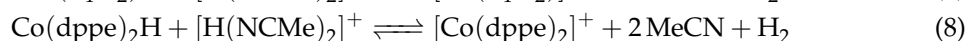
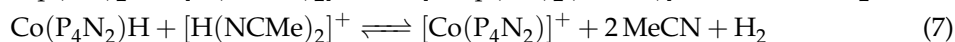
Implicit solvation is used as a way to approximate the solvation of gas phase molecules, with continuum models used to describe a solvation shell around a molecule as a dielectric; however, this does not describe specific interactions, where a solvent molecule may act as a ligand to stabilise an ionic species (Equation (4)). In such cases, the explicit treatment of a solvent molecule is required to describe the role as a ligand in the coordination sphere and

as such, the reaction shown in Equation (2) may be better represented by the reaction in Equation (5), where both cations are solvated by explicit solvent molecules.



If a solvent molecule is coordinated to the metal centre after hydride dissociation, according to Equation (1), this binding energy is implicitly included in the experimental determination of thermodynamic hydricity by Wiedner et al. [39] (Equation (2)). Across the three complexes used (Table 2), both the sterics and accessibility of the solvent to the coordination shell are significantly different. In cationic metal complexes, where a vacant coordination site is exposed and accessible, a solvent molecule may strongly bind to the metal centre, stabilising the complex to a higher degree than would be predicted with only the inclusion of a dielectric model. Here, the bond dissociation energy of the ligand (Equation (4)) becomes important and a solvent molecule should be treated explicitly if there is a strong interaction between the cationic metal complex and solvent molecule.

The Fe cationic complex has a low steric bulk and vacant and accessible coordination sphere,  $[\text{FeCp}(\text{CO})_2]^+$ . In contrast, the two Co complexes have large ligands attached to each metal centre and are far more sterically crowded (see 3D surface plots in Table 2). We found that, for the most accurate computed hydricity values, the Fe cationic species must be treated with an explicitly bound solvent molecule, whereas the Co complexes do not require this (Equations (6)–(8)). While there is an element of functional dependence, this methodology has been tested and was found to produce the lowest mean absolute errors (MAEs) in the calculation of hydricity when compared to the values obtained by Wiedner et al. [39] (further details are available in Section 3 of the ESI).



### 3.2. Choice of Single-Point Functional

To quantitatively predict the thermodynamic hydricity of a complex, the ability of the functional used to produce accurate energies is of prime importance. Single-point energy calculations have been performed with a range of functionals, on geometry optimised structures at the level of RI-BP86-D3( $\text{PCM}_{\text{MeCN}}$ ), with a large triple- $\zeta$  basis, def2-TZVP, from the group of Ahlrichs [40–43].

The functional used in the single-point calculation was found to have a significant impact upon the ability to quantitatively reproduce thermodynamic hydricity values obtained from experiment. Errors in the form of mean absolute error, have been calculated for each functional across the three complexes (Equation (9) and Figure 1).

$$\text{MAE} = \frac{1}{n} \sum |E_{\text{calc}} - E_{\text{exp}}| \quad (9)$$

Clearly, the Minnesota functionals of M06-2X and M06-HF, both highly parameterised for main group chemistry, are poor in their description of these 3d TM complexes. The lowest MAEs were obtained from RI-BP86, PBE0 and revPBE0 (1.7, 1.3 and 0.9 kcal/mol). The percentage of HF exchange has been shown to be important by Moltved et al. [83] and this effect can be seen in the comparison of PBE0 with PBE0-1/3, with 25% and 33% HF exchange, respectively. Both forms of the hybrid PBE functional performed well in terms of overall performance, yet PBE0-1/3 had over twice the MAE of PBE0 (1.3 and 2.9 kcal/mol, respectively).

Based purely upon the MAEs obtained here, revPBE0 would be the functional of choice; however, we recommend to use PBE0 (based upon an improved performance over revPBE0 on geometries produced with the smaller def2-SVP basis, MAEs of 1.4 and

1.8 kcal/mol, see ESI Figure S7 and Section 3.3.2), which has been shown to perform well in many previous studies of TM systems [17,85] and in the differentiation of spin state energetics [17].

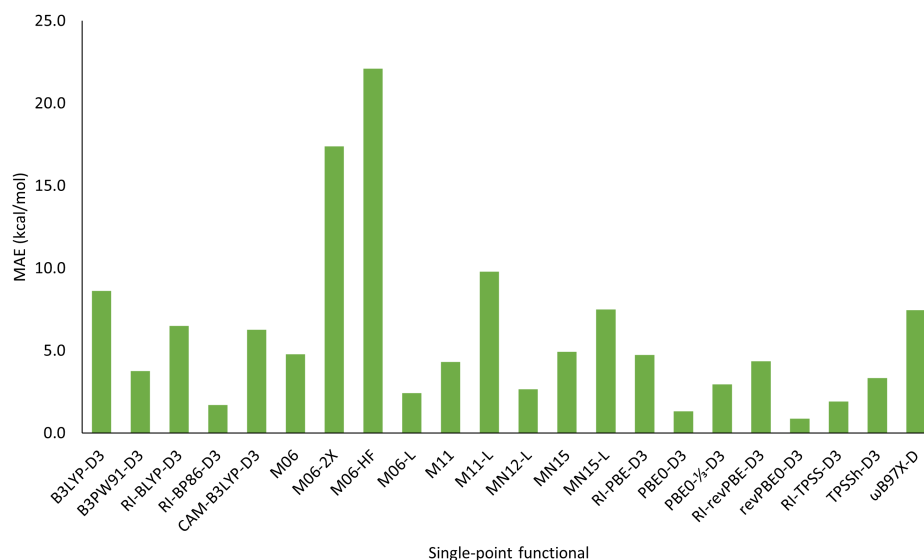


**Figure 1.** MAE in the calculation of hydricity across each of the three complexes with a range of single-point functionals. Performed with implicit solvation ( $\text{PCM}_{\text{MeCN}}$ ) and a def2-TZVP basis on optimised geometries from RI-BP86-D3( $\text{PCM}_{\text{MeCN}}$ )/def2-TZVP.

### 3.3. Validation of Methodology

We have carefully tested the robustness of the benchmark data summarised in Figure 1 against other choices of methodological details. These comprise:

#### 3.3.1. Choice of Basis Set for Single-Point Energies

Single-point calculations in this work were performed using the def2-TZVP basis from Ahlrichs. The impact of a larger, quadruple- $\zeta$  basis, def2-QZVP, was examined on the smallest Fe system for a selection of single-points (Figure S4 in the ESI).

For the additional expense of using a quadruple- $\zeta$  basis in the description of the system, there was no significant improvement to be found. Def2-TZVP has been shown to be of sufficient accuracy for single-point calculations and a greater emphasis is placed upon the choice of functional for these 3d TM hydride complexes.

#### 3.3.2. Level of Geometry Optimisation

RI-BP86 was initially chosen for use in geometry optimisation as a ‘tried and tested’ method [48]. From comparison of BP86 with PBE0, M06 and M06-L, it was found that there was no benefit to the use of the more expensive hybrid, meta-hybrid or meta-GGA functional over the pure functional in the geometry optimisation (MAEs of 1.4, 4.8, 4.5 and 4.3 kcal/mol, respectively, Figure S5 in the ESI).

Furthermore, under consideration was the use of a different basis in the optimisation. In general, use of the largest, triple- $\zeta$ , def2-TZVP basis set was found to perform best, with a reduction in MAE compared to the smaller double- $\zeta$ , def2-SVP basis. Though, we did find that the description of the hydridic hydrogen with an additional diffuse function, or of the metal centre with a larger basis, was not always found to improve the MAE (see Figure S7 in the ESI). While the triple- $\zeta$  basis was found to offer a slight improvement, the associated expense of using this larger basis means that this is impractical for the fractional improvement and the smaller, double- $\zeta$  basis is deemed sufficient for geometry optimisation of these systems (MAEs of 1.3 and 1.4 kcal/mol, respectively, from single-points of PBE0-D3( $\text{PCM}_{\text{MeCN}}$ )/def2-TZVP, but with CPU times for the frequency calculation, at the level of

geometry optimisation, for  $\text{Co}(\text{dppe})_2\text{H}$  of approximately 12.5 days compared to 2 days for def2-TZVP and def2-SVP basis sets, respectively). Additionally, there was little change in the optimised geometry between the use of def2-SVP and def2-TZVP, with central metal ligand and bond distances reproduced to within 0.006 Å (see Table S3 in the ESI for a comparison to X-Ray crystal structures from Ciancanelli et al. [81] and Ariyaratne et al. [86]).

Theoretically, for the most accurate description of the system, both dispersion and solvation should be considered and indeed we found that the inclusion of both minimised the MAEs in the calculation of hydricity across the three complexes (Figure S8 in the ESI).

### 3.3.3. Choice of Solvation Model

The choice of solvent model has been examined at the level of single-point calculations and there was no significant variation of the hydricity values obtained by using three different solvation models; IEF-PCM, C-PCM and SMD (Table S4 in the ESI).

## 4. Conclusions

We have accurately reproduced experimentally measured values of hydricity for three 3d TM complexes. While a mixture of functionals have been used in the literature for studies on 3d metal homogeneous catalysis, we propose a methodology that has been shown to accurately reproduce a key M–H bond strength, central to the reactivity of these compounds.

While low on the Jacob's ladder of functionals, the pure GGA, BP86, has been shown to produce accurate energetics for the hydricity of 3d TM hydrides. The hybrid functional, PBE0 has also been shown to perform well and is recommended for energy calculations over BP86 due to the improved ability to more reliably differentiate between spin states of 3d TM complexes [17]. The lowest mean absolute errors were found with the inclusion of both dispersion corrections and implicit solvation.

A double- $\zeta$  basis, def2-SVP, was used in geometry optimisation with the RI-BP86-D3(PCM) and led to a MAE of 1.4 kcal/mol after evaluation of subsequent single-point at the level of PBE0-D3(PCM)/def2-TZVP. A larger triple- $\zeta$  basis, def2-TZVP, used at the stage of the geometry optimisation led to a lower MAE of 1.3 kcal/mol which, was not shown to offer any significant improvement for the additional cost.

For a balance between accuracy and expense, we recommend the methodology of PBE0-D3(PCM)/def2-TZVP//RI-BP86-D3(PCM)/def2-SVP for use on systems involving 3d TM hydride complexes.

**Supplementary Materials:** The following are available online at, additional computational details and graphical and tabular material.

**Author Contributions:** Conceptualisation, M.B.; methodology, A.S.G. and M.B.; investigation, A.S.G.; writing—original draft, A.S.G.; Supervision, M.B. All authors have read and agreed to the published version of the manuscript.

**Funding:** This research received no external funding. The publication of this work received support from the St Andrews Institutional Open Access Fund.

**Institutional Review Board Statement:** Not applicable.

**Informed Consent Statement:** Not applicable.

**Data Availability Statement:** The research data supporting this publication can be accessed at <https://doi.org/10.17630/7cf7b7e9-3edc-4ad4-b016-3b9b5548f9ac> (accessed on 2 July 2021).

**Acknowledgments:** We thank EastCHEM and the School of Chemistry for support through the EaSI-CAT program. Calculations were performed on a local compute cluster maintained by H. Früchtl.

**Conflicts of Interest:** The authors declare no conflict of interest.

## References

1. Herrmann, W.A.; Cornils, B. Organometallic Homogeneous Catalysis - Quo vadis? *Angew. Chem. (Int. Ed. Engl.)* **1997**, *36*, 1048–1067. [[CrossRef](#)]
2. Reed-Berendt, B.G.; Polidano, K.; Morrill, L.C. Recent advances in homogeneous borrowing hydrogen catalysis using earth-abundant first row transition metals. *Org. Biomol. Chem.* **2019**, *17*, 1595–1607. [[CrossRef](#)]
3. Carney, J.R.; Dillon, B.R.; Thomas, S.P. Recent Advances of Manganese Catalysis for Organic Synthesis. *Eur. J. Org. Chem.* **2016**, *2016*, 3912–3929. [[CrossRef](#)]
4. Mukherjee, A.; Milstein, D. Homogeneous Catalysis by Cobalt and Manganese Pincer Complexes. *ACS Catal.* **2018**, *8*, 11435–11469. [[CrossRef](#)]
5. Bender, T.A.; Dabrowski, J.A.; Gagné, M.R. Homogeneous catalysis for the production of low-volume, high-value chemicals from biomass. *Nat. Rev. Chem.* **2018**, *2*, 35–46. [[CrossRef](#)]
6. Garbe, M.; Junge, K.; Beller, M. Homogeneous Catalysis by Manganese-Based Pincer Complexes. *Eur. J. Org. Chem.* **2017**, *2017*, 4344–4362. [[CrossRef](#)]
7. Cramer, C.J.; Truhlar, D.G. Density functional theory for transition metals and transition metal chemistry. *Phys. Chem. Chem. Phys.* **2009**, *11*, 10757–10816. [[CrossRef](#)]
8. Vogiatzis, K.D.; Polynski, M.V.; Kirkland, J.K.; Townsend, J.; Hashemi, A.; Liu, C.; Pidko, E.A. Computational Approach to Molecular Catalysis by 3d Transition Metals: Challenges and Opportunities. *Chem. Rev.* **2019**, *119*, 2453–2523. [[CrossRef](#)] [[PubMed](#)]
9. Elangovan, S.; Topf, C.; Fischer, S.; Jiao, H.; Spannenberg, A.; Baumann, W.; Ludwig, R.; Junge, K.; Beller, M. Selective Catalytic Hydrogenations of Nitriles, Ketones, and Aldehydes by Well-Defined Manganese Pincer Complexes. *J. Am. Chem. Soc.* **2016**, *138*, 8809–8814. [[CrossRef](#)]
10. Wei, Z.; De Aguirre, A.; Junge, K.; Beller, M.; Jiao, H. Exploring the mechanisms of aqueous methanol dehydrogenation catalyzed by defined PNP Mn and Re pincer complexes under base-free as well as strong base conditions. *Catal. Sci. Technol.* **2018**, *8*, 3649–3665. [[CrossRef](#)]
11. Junge, K.; Wendt, B.; Jiao, H.; Beller, M. Iridium-Catalyzed Hydrogenation of Carboxylic Acid Esters. *ChemCatChem* **2014**, *6*, 2810–2814. [[CrossRef](#)]
12. Wei, Z.; Junge, K.; Beller, M.; Jiao, H. Hydrogenation of phenyl-substituted CN, CN, CC, CC and CO functional groups by Cr, Mo and W PNP pincer complexes—A DFT study. *Catal. Sci. Technol.* **2017**, *7*, 2298–2307. [[CrossRef](#)]
13. Alberico, E.; Lennox, A.J.; Vogt, L.K.; Jiao, H.; Baumann, W.; Drexler, H.J.; Nielsen, M.; Spannenberg, A.; Checinski, M.P.; Junge, H.; et al. Unravelling the Mechanism of Basic Aqueous Methanol Dehydrogenation Catalyzed by Ru-PNP Pincer Complexes. *J. Am. Chem. Soc.* **2016**, *138*, 14890–14904. [[CrossRef](#)]
14. Jiao, H.; Junge, K.; Alberico, E.; Beller, M. A Comparative Computationally Study About the Defined M(II) Pincer Hydrogenation Catalysts (M = Fe, Ru, Os). *J. Comput. Chem.* **2016**, *37*, 168–176. [[CrossRef](#)] [[PubMed](#)]
15. Elangovan, S.; Garbe, M.; Jiao, H.; Spannenberg, A.; Junge, K.; Beller, M. Hydrogenation of Esters to Alcohols Catalyzed by Defined Manganese Pincer Complexes. *Angew. Chem.* **2016**, *128*, 15590–15594. [[CrossRef](#)]
16. Ge, H.; Chen, X.; Yang, X. A mechanistic study and computational prediction of iron, cobalt and manganese cyclopentadienone complexes for hydrogenation of carbon dioxide. *Chem. Commun.* **2016**, *52*, 12422–12425. [[CrossRef](#)]
17. Gámez, J.A.; Hölscher, M.; Leitner, W. On the applicability of density functional theory to manganese-based complexes with catalytic activity toward water oxidation. *J. Comput. Chem.* **2017**, *38*, 1747–1751. [[CrossRef](#)] [[PubMed](#)]
18. Qian, F.; Chen, X.; Yang, X. DFT and AIMD prediction of a SNS manganese pincer complex for hydrogenation of acetophenone. *Chem. Phys. Lett.* **2019**, *714*, 37–44. [[CrossRef](#)]
19. Chen, X.; Ge, H.; Yang, X. Newly designed manganese and cobalt complexes with pendant amines for the hydrogenation of CO<sub>2</sub> to methanol: A DFT study. *Catal. Sci. Technol.* **2017**, *7*, 348–355. [[CrossRef](#)]
20. Passera, A.; Mezzetti, A. Mn(I) and Fe(II)/PN(H)P Catalysts for the Hydrogenation of Ketones: A Comparison by Experiment and Calculation. *Adv. Synth. Catal.* **2019**, *361*, 4691–4706. [[CrossRef](#)]
21. Zubar, V.; Lebedev, Y.; Azofra, L.M.; Cavallo, L.; El-Sepelgy, O.; Rueping, M. Hydrogenation of CO<sub>2</sub>-Derived Carbonates and Polycarbonates to Methanol and Diols by Metal–Ligand Cooperative Manganese Catalysis. *Angew. Chem. Int. Ed.* **2018**, *57*, 13439–13443. [[CrossRef](#)]
22. Garbe, M.; Junge, K.; Walker, S.; Wei, Z.; Jiao, H.; Spannenberg, A.; Bachmann, S.; Scalone, M.; Beller, M. Manganese(I)-Catalyzed Enantioselective Hydrogenation of Ketones Using a Defined Chiral PNP Pincer Ligand. *Angew. Chem.* **2017**, *129*, 11389–11393. [[CrossRef](#)]
23. Zhang, L.; Wang, Z.; Han, Z.; Ding, K. Manganese-Catalyzed anti-Selective Asymmetric Hydrogenation of  $\alpha$ -Substituted  $\beta$ -Ketoamides. *Angew. Chem.* **2020**, *132*, 15695–15699. [[CrossRef](#)]
24. Wang, Y.; Zhu, L.; Shao, Z.; Li, G.; Lan, Y.; Liu, Q. Unmasking the Ligand Effect in Manganese-Catalyzed Hydrogenation: Mechanistic Insight and Catalytic Application. *J. Am. Chem. Soc.* **2019**, *141*, 17337–17349. [[CrossRef](#)]
25. Glatz, M.; Stöger, B.; Himmelbauer, D.; Veiros, L.F.; Kirchner, K. Chemoselective Hydrogenation of Aldehydes under Mild, Base-Free Conditions: Manganese Outperforms Rhenium. *ACS Catal.* **2018**, *8*, 4009–4016. [[CrossRef](#)]

26. Van Putten, R.; Uslamin, E.A.; Garbe, M.; Liu, C.; Gonzalez-de Castro, A.; Lutz, M.; Junge, K.; Hensen, E.J.; Beller, M.; Lefort, L.; et al. Non-Pincer-Type Manganese Complexes as Efficient Catalysts for the Hydrogenation of Esters. *Angew. Chem. Int. Ed.* **2017**, *56*, 7531–7534. [[CrossRef](#)]
27. Ryabchuk, P.; Stier, K.; Junge, K.; Checinski, M.P.; Beller, M. Molecularly Defined Manganese Catalyst for Low-Temperature Hydrogenation of Carbon Monoxide to Methanol. *J. Am. Chem. Soc.* **2019**, *141*, 16923–16929. [[CrossRef](#)] [[PubMed](#)]
28. Zeng, L.; Yang, H.; Zhao, M.; Wen, J.; Tucker, J.H.; Zhang, X. C1-Symmetric PNP Ligands for Manganese-Catalyzed Enantioselective Hydrogenation of Ketones: Reaction Scope and Enantioinduction Model. *ACS Catal.* **2020**, *10*, 13794–13799. [[CrossRef](#)]
29. Liu, C.; van Putten, R.; Kulyaev, P.O.; Filonenko, G.A.; Pidko, E.A. Computational insights into the catalytic role of the base promoters in ester hydrogenation with homogeneous non-pincer-based Mn-P,N catalyst. *J. Catal.* **2018**, *363*, 136–143. [[CrossRef](#)]
30. Van Putten, R.; Filonenko, G.A.; Gonzalez De Castro, A.; Liu, C.; Weber, M.; Müller, C.; Lefort, L.; Pidko, E. Mechanistic Complexity of Asymmetric Transfer Hydrogenation with Simple Mn-Diamine Catalysts. *Organometallics* **2019**, *38*, 3187–3196. [[CrossRef](#)]
31. Zirakzadeh, A.; de Aguiar, S.R.; Stöger, B.; Widhalm, M.; Kirchner, K. Enantioselective Transfer Hydrogenation of Ketones Catalyzed by a Manganese Complex Containing an Unsymmetrical Chiral PNP' Tridentate Ligand. *ChemCatChem* **2017**, *9*, 1744–1748. [[CrossRef](#)]
32. Rawat, K.S.; Mahata, A.; Choudhuri, I.; Pathak, B. Catalytic hydrogenation of CO<sub>2</sub> by manganese complexes: Role of  $\pi$ -acceptor ligands. *J. Phys. Chem. C* **2016**, *120*, 16478–16488. [[CrossRef](#)]
33. Yang, X. Hydrogenation of carbon dioxide catalyzed by PNP pincer iridium, iron, and cobalt complexes: A computational design of base metal catalysts. *ACS Catal.* **2011**, *1*, 849–854. [[CrossRef](#)]
34. Mondal, B.; Sengupta, K.; Rana, A.; Mahammed, A.; Botoshansky, M.; Dey, S.G.; Gross, Z.; Dey, A. Cobalt corrole catalyst for efficient hydrogen evolution reaction from H<sub>2</sub>O under ambient conditions: Reactivity, spectroscopy, and density functional theory calculations. *Inorg. Chem.* **2013**, *52*, 3381–3387. [[CrossRef](#)] [[PubMed](#)]
35. Ganguly, G.; Malakar, T.; Paul, A. Theoretical studies on the mechanism of homogeneous catalytic olefin hydrogenation and amine-borane dehydrogenation by a versatile boryl-ligand-based cobalt catalyst. *ACS Catal.* **2015**, *5*, 2754–2769. [[CrossRef](#)]
36. Della Monica, F.; Vummaleti, S.V.; Buonerba, A.; Nisi, A.D.; Monari, M.; Milione, S.; Grassi, A.; Cavallo, L.; Capacchione, C. Coupling of Carbon Dioxide with Epoxides Efficiently Catalyzed by Thioether-Triphenolate Bimetallic Iron(III) Complexes: Catalyst Structure–Reactivity Relationship and Mechanistic DFT Study. *Adv. Synth. Catal.* **2016**, *358*, 3231–3243. [[CrossRef](#)]
37. Murugesan, K.; Wei, Z.; Chandrashekhar, V.G.; Neumann, H.; Spannenberg, A.; Jiao, H.; Beller, M.; Jagadeesh, R.V. Homogeneous cobalt-catalyzed reductive amination for synthesis of functionalized primary amines. *Nat. Commun.* **2019**, *10*, 1–9. [[CrossRef](#)] [[PubMed](#)]
38. Li, Y.Y.; Tong, L.P.; Liao, R.Z. Mechanism of Water Oxidation Catalyzed by a Mononuclear Iron Complex with a Square Polypyridine Ligand: A DFT Study. *Inorg. Chem.* **2018**, *57*, 4590–4601. [[CrossRef](#)] [[PubMed](#)]
39. Wiedner, E.S.; Chambers, M.B.; Pitman, C.L.; Bullock, R.M.; Miller, A.J.; Appel, A.M. Thermodynamic Hydricity of Transition Metal Hydrides. *Chem. Rev.* **2016**, *116*, 8655–8692. [[CrossRef](#)]
40. Schäfer, A.; Horn, H.; Ahlrichs, R. Fully optimized contracted Gaussian basis sets for atoms Li to Kr. *J. Chem. Phys.* **1992**, *97*, 2571–2577. [[CrossRef](#)]
41. Schäfer, A.; Huber, C.; Ahlrichs, R. Fully optimized contracted Gaussian basis sets of triple zeta valence quality for atoms Li to Kr. *J. Chem. Phys.* **1994**, *100*, 5829–5835. [[CrossRef](#)]
42. Weigend, F.; Ahlrichs, R. Balanced basis sets of split valence, triple zeta valence and quadruple zeta valence quality for H to Rn: Design and assessment of accuracy. *Phys. Chem. Chem. Phys.* **2005**, *7*, 3297–3305. [[CrossRef](#)] [[PubMed](#)]
43. Weigend, F. Accurate Coulomb-fitting basis sets for H to Rn. *Phys. Chem. Chem. Phys.* **2006**, *8*, 1057–1065. [[CrossRef](#)] [[PubMed](#)]
44. Chin, B.; Lough, A.J.; Morris, R.H.; Schweitzer, C.T.; D'Agostino, C. Influence of Chloride versus Hydride on H-H Bonding and Acidity of the Trans Dihydrogen Ligand in the Complexes trans-[Ru(H<sub>2</sub>)X(PR<sub>2</sub>CH<sub>2</sub>CH<sub>2</sub>PR<sub>2</sub>)<sub>2</sub>]<sup>+</sup>, X = Cl, H, R = Ph, Et. Crystal Structure Determinations of [RuCl(dppe)<sub>2</sub>]PF<sub>6</sub> and trans-[Ru(H<sub>2</sub>)Cl(dppe)<sub>2</sub>]PF<sub>6</sub>. *Inorg. Chem.* **1994**, *33*, 6278–6288. [[CrossRef](#)]
45. Guerchais, V.; Astruc, D.; Nunn, C.M.; Cowley, A.H. Generation, Characterization, and Chemistry of the Methylene Complexes [Fe( $\eta^5$ -C<sub>5</sub>Me<sub>5</sub>)(CO)(L)(=CH<sub>2</sub>)]<sup>+</sup> (L = CO, PPh<sub>3</sub>) and the X-ray Crystal Structure of [Fe( $\eta^5$ -C<sub>5</sub>Me<sub>5</sub>)(CO)<sub>2</sub>(CH<sub>2</sub>PPh<sub>3</sub>)]<sup>+</sup>BF<sub>4</sub><sup>-</sup>. *Organometallics* **1990**, *9*, 1036–1041. [[CrossRef](#)]
46. Klug, C.M.; Dougherty, W.G.; Kassel, W.S.; Wiedner, E.S. Electrocatalytic Hydrogen Production by a Nickel Complex Containing a Tetradentate Phosphine Ligand. *Organometallics* **2019**, *38*, 1269–1279. [[CrossRef](#)]
47. Neale, S.E. Computational Investigations of Homogeneous Catalysis and Spin- State Energetics in Fe ( II ) and Co ( III ) Complexes. Ph.D. Thesis, Heriot-Watt University, Edinburgh, UK, 2019.
48. Bühl, M.; Kabrede, H. Geometries of transition-metal complexes from density-functional theory. *J. Chem. Theory Comput.* **2006**, *2*, 1282–1290. [[CrossRef](#)]
49. Grimme, S.; Antony, J.; Ehrlich, S.; Krieg, H. A consistent and accurate ab initio parametrization of density functional dispersion correction (DFT-D) for the 94 elements H-Pu. *J. Chem. Phys.* **2010**, *132*, 154104. [[CrossRef](#)]
50. Grimme, S.; Ehrlich, S.; Goerigk, L. Effect of the Damping Function in Dispersion Corrected Density Functional Theory. *J. Comput. Chem.* **2011**, *32*, 1457–1465. [[CrossRef](#)]
51. Perdew, J.P.; Ruzsinszky, A.; Tao, J.; Staroverov, V.N.; Scuseria, G.E.; Csonka, G.I. Prescription for the design and selection of density functional approximations: More constraint satisfaction with fewer fits. *J. Chem. Phys.* **2005**, *123*, 062201. [[CrossRef](#)]

52. Becke, A.D. Density-functional thermochemistry. III. The role of exact exchange. *J. Chem. Phys.* **1993**, *98*, 5648–5652. [[CrossRef](#)]
53. Lee, C.; Yang, W.; Parr, R.G. Development of the Colle-Salvetti correlation-energy formula into a functional of the electron density. *Phys. Rev. B* **1988**, *37*, 785–789. [[CrossRef](#)] [[PubMed](#)]
54. Miehlich, B.; Savin, A.; Stoll, H.; Preuss, H. Results obtained with the correlation energy density functionals of Becke and Lee, Yang and Parr. *Chem. Phys. Lett.* **1989**, *157*, 200–206. [[CrossRef](#)]
55. Perdew, J.P.; Burke, K.; Wang, Y. Generalized gradient approximation for the exchange-correlation hole of a many-electron system. *Phys. Rev. B* **1996**, *54*, 16533–16539. [[CrossRef](#)]
56. Perdew, J.P.; Chevary, J.A.; Vosko, S.H.; Jackson, K.A.; Pederson, M.R.; Singh, D.J.; Fiolhais, C. Atoms, molecules, solids, and surfaces: Applications of the generalized gradient approximation for exchange and correlation. *Phys. Rev. B* **1992**, *46*, 6671–6687. [[CrossRef](#)] [[PubMed](#)]
57. Shi, J.M.; Peeters, F.M.; Hai, G.Q.; Devreese, J.T. Erratum: Donor transition energy in GaAs superlattices in a magnetic field along the growth axis. *Phys. Rev. B* **1993**, *48*, 4978–4978. [[CrossRef](#)] [[PubMed](#)]
58. Becke, A.D. Density-functional exchange-energy approximation with correct asymptotic behaviour. *Phys. Rev. A* **1988**, *38*, 3098–3100. [[CrossRef](#)] [[PubMed](#)]
59. Perdew, J.P. Density-functional approximation for the correlation energy of the inhomogeneous electron gas. *Phys. Rev. B* **1986**, *33*, 8822–8824. [[CrossRef](#)]
60. Yanai, T.; Tew, D.P.; Handy, N.C. A new hybrid exchange-correlation functional using the Coulomb-attenuating method (CAM-B3LYP). *Chem. Phys. Lett.* **2004**, *393*, 51–57. [[CrossRef](#)]
61. Zhao, Y.; Truhlar, D.G. The M06 suite of density functionals for main group thermochemistry, thermochemical kinetics, noncovalent interactions, excited states, and transition elements: Two new functionals and systematic testing of four M06-class functionals and 12 other function. *Theor. Chem. Acc.* **2008**, *120*, 215–241. [[CrossRef](#)]
62. Zhao, Y.; Truhlar, D.G. Comparative DFT study of van der Waals complexes: Rare-gas dimers, alkaline-earth dimers, zinc dimer and zinc-rare-gas dimers. *J. Phys. Chem. A* **2006**, *110*, 5121–5129. [[CrossRef](#)] [[PubMed](#)]
63. Zhao, Y.; Truhlar, D.G. Density functional for spectroscopy: No long-range self-interaction error, good performance for Rydberg and charge-transfer states, and better performance on average than B3LYP for ground states. *J. Phys. Chem. A* **2006**, *110*, 13126–13130. [[CrossRef](#)] [[PubMed](#)]
64. Zhao, Y.; Truhlar, D.G. A new local density functional for main-group thermochemistry, transition metal bonding, thermochemical kinetics, and noncovalent interactions. *J. Chem. Phys.* **2006**, *125*, 194101. [[CrossRef](#)] [[PubMed](#)]
65. Peverati, R.; Truhlar, D.G. Improving the accuracy of hybrid meta-GGA density functionals by range separation. *J. Phys. Chem. Lett.* **2011**, *2*, 2810–2817. [[CrossRef](#)]
66. Peverati, R.; Truhlar, D.G. M11-L: A local density functional that provides improved accuracy for electronic structure calculations in chemistry and physics. *J. Phys. Chem. Lett.* **2012**, *3*, 117–124. [[CrossRef](#)]
67. Peverati, R.; Truhlar, D.G. An improved and broadly accurate local approximation to the exchange-correlation density functional: The MN12-L functional for electronic structure calculations in chemistry and physics. *Phys. Chem. Chem. Phys.* **2012**, *14*, 13171–13174. [[CrossRef](#)]
68. Yu, H.S.; He, X.; Li, S.L.; Truhlar, D.G. MN15: A Kohn-Sham global-hybrid exchange-correlation density functional with broad accuracy for multi-reference and single-reference systems and noncovalent interactions. *Chem. Sci.* **2016**, *7*, 5032–5051. [[CrossRef](#)]
69. Yu, H.S.; He, X.; Truhlar, D.G. MN15-L: A New Local Exchange-Correlation Functional for Kohn-Sham Density Functional Theory with Broad Accuracy for Atoms, Molecules, and Solids. *J. Chem. Theory Comput.* **2016**, *12*, 1280–1293. [[CrossRef](#)] [[PubMed](#)]
70. Perdew, J.P.; Burke, K.; Ernzerhof, M. Errata: Generalized Gradient Approximation Made Simple [Phys. Rev. Lett. *77*, 3865 (1996)]. *Phys. Rev. Lett.* **1997**, *78*, 1396. [[CrossRef](#)]
71. Adamo, C.; Barone, V. Toward reliable density functional methods without adjustable parameters: The PBE0 model. *J. Chem. Phys.* **1999**, *110*, 6158–6170. [[CrossRef](#)]
72. Guido, C.A.; Brémond, E.; Adamo, C.; Cortona, P. Communication: One third: A new recipe for the PBE0 paradigm. *J. Chem. Phys.* **2013**, *138*, 021104. [[CrossRef](#)]
73. Ernzerhof, M.; Perdew, J.P. Generalized gradient approximation to the angle- and system-averaged exchange hole. *J. Chem. Phys.* **1998**, *109*, 3313–3320. [[CrossRef](#)]
74. Tao, J.; Perdew, J.P.; Staroverov, V.N.; Scuseria, G.E. Climbing the density functional ladder: Nonempirical meta-generalized gradient approximation designed for molecules and solids. *Phys. Rev. Lett.* **2003**, *91*, 146401. [[CrossRef](#)]
75. Staroverov, V.N.; Scuseria, G.E.; Tao, J.; Perdew, J.P. Comparative assessment of a new nonempirical density functional: Molecules and hydrogen-bonded complexes. *J. Chem. Phys.* **2003**, *119*, 12129–12137; Erratum in *J. Chem. Phys.* **2004**, *121*, 11507. [[CrossRef](#)]
76. Chai, J.D.; Head-Gordon, M. Long-range corrected hybrid density functionals with damped atom-atom dispersion corrections. *Phys. Chem. Chem. Phys.* **2008**, *10*, 6615–6620. [[CrossRef](#)]
77. Grimme, S. Semiempirical GGA-Type Density Functional Constructed with a Long-Range Dispersion Correction. *J. Comput. Chem.* **2006**, *27*, 1787–1799. [[CrossRef](#)]
78. Frisch, M.J.; Trucks, G.W.; Schlegel, H.B.; Scuseria, G.E.; Robb, M.A.; Cheeseman, J.R.; Scalmani, G.; Barone, V.; Mennucci, B.; Petersson, G.A.; et al. *Gaussian 09, Revision D.01*; Gaussian Inc.: Wallingford, CT, USA, 2013.
79. Frisch, M.J.; Trucks, G.W.; Schlegel, H.B.; Scuseria, G.E.; Robb, M.A.; Cheeseman, J.R.; Scalmani, G.; Barone, V.; Petersson, G.A.; Nakatsuji, H.; et al. *Gaussian 16, Revision C.01*; Gaussian Inc.: Wallingford, CT, USA, 2019.

80. Estes, D.P.; Vannucci, A.K.; Hall, A.R.; Lichtenberger, D.L.; Norton, J.R. Thermodynamics of the metal-hydrogen bonds in  $(\eta^5\text{-C}_5\text{H}_5)\text{M}(\text{CO})_2\text{H}$  (M = Fe, Ru, Os). *Organometallics* **2011**, *30*, 3444–3447. [[CrossRef](#)]
81. Ciancanelli, R.; Noll, B.C.; DuBois, D.L.; Rakowski DuBois, M. Comprehensive thermodynamic characterization of the metal-hydrogen bond in a series of cobalt-hydride complexes. *J. Am. Chem. Soc.* **2002**, *124*, 2984–2992. [[CrossRef](#)]
82. Wiedner, E.S.; Appel, A.M.; Dubois, D.L.; Bullock, R.M. Thermochemical and mechanistic studies of electrocatalytic hydrogen production by cobalt complexes containing pendant amines. *Inorg. Chem.* **2013**, *52*, 14391–14403. [[CrossRef](#)] [[PubMed](#)]
83. Moltved, K.A.; Kepp, K.P. Chemical Bond Energies of 3d Transition Metals Studied by Density Functional Theory. *J. Chem. Theory Comput.* **2018**, *14*, 3479–3492. [[CrossRef](#)] [[PubMed](#)]
84. Himmel, D.; Goll, S.K.; Leito, I.; Krossing, I. A unified pH scale for all phases. *Angew. Chem. Int. Ed.* **2010**, *49*, 6885–6888. [[CrossRef](#)] [[PubMed](#)]
85. Bühl, M.; Reimann, C.; Pantazis, D.A.; Bredow, T.; Neese, F. Geometries of third-row transition-metal complexes from density-functional theory. *J. Chem. Theory Comput.* **2008**, *4*, 1449–1459. [[CrossRef](#)] [[PubMed](#)]
86. Ariyaratne, J.K.P.; Bierrum, A.M.; Green, M.L.H.; Ishaq, M.; Prout, C.K.; Swanwick, M.G. Evidence for near-neighbour interactions in some substituted methyl derivatives of transition metals including the molecular crystal structure determinations of  $(\pi\text{-C}_5\text{H}_5)\text{Fe}(\text{CO})_2\text{CH}_2\text{CO}_2\text{H}$  and  $(\pi\text{-C}_5\text{H}_5)\text{Mo}(\text{CO})_3\text{CH}_2\text{CO}_2\text{H}$ . *J. Chem. Soc. A* **1969**, 1309–1321. [[CrossRef](#)]